

SIMULATIONS OF A LIQUID BILAYER AND HUNT FOR PROTRUSIONS.

by
J. Stecki

Department III, Institute of Physical Chemistry,
Polish Academy of Sciences,
ul. Kasprzaka 44/52, 01-224 Warszawa, Poland

November 17, 2018

Abstract.

New simulations are reported of a single bilayer immersed in a liquid solvent, using a simple extension of the model of the Max-Planck group as used in earlier work. Fluctuation spectrum *vel* structure factor is dissected in detail and the role of bulk fluctuations is revealed.. We propose to search for protrusions directly where they are, *i.e.* at the solvent-head boundary. In this context new single-point quantities and new two-point correlations are introduced and determined for the solvent-head pairs. Most unusual shapes are obtained.

Introduction.

Simulations of liquid bilayers have been numerous and helpful in understanding their properties[1][2]. In one particular line of research the structure factor $S(q)$, readily determined in the simulation, is examined. For extended bilayers under lateral tension, S shows the $1/q^2$ divergence as the transverse Fourier vector \mathbf{q} approaches zero. It is a manifestation of the celebrated Goldstone mode and the capillary-wave undulations related to it. This capillary-wave contribution, augmented as it may be by a $1/q^4$ term, dies quickly with raising q .

Beyond that divergence, the fluctuation spectrum *vel* structure factor is not widely nor fully understood. There is present, as must be, some contribution from local compression-dilatation processes present in all liquids as density fluctuations. Also, the polar heads in contact with the (polar) solvent may not make a perfect plane but may "protrude" into the solvent. The morphology of such "protrusions" and the dynamics of their formation is not known and has not been determined in any simulation. But otherwise it has been convincingly shown theoretically[3] that the protrusions, if indeed they exist, ought to modify the hydrophobic repulsion between adjacent bilayers in a lamellar stack. In the stack, bilayers are separated by layers of water - whose thickness d defines various regimes of the physics of the lamellae. The hydrophobic repulsion has been measured in the laboratory and its exponential decay with d is established.

For such reasons, search for protrusions is desirable and much needed. We do that in a new way. We propose to look directly for protrusions where they are, *i.e.* at the solvent-head boundary.

But first we examine further the structure factor $S(q)$ defined as the height-height correlation function. (Section 1). As we have emphasized long time ago[4,5] it is necessary to go beyond the asymptotic region of the capillary wave divergence and examine a wider range of the Fourier variable q . Then the nearest-neighbor peak appears[4][6].

In the search for protrusions we introduced some novel quantities, which are shown in Section 2. But above all, instead of searching for their presence in $S(q)$, we attempted to find them "where they are" and that was met with success.

The model we use for simulations has been introduced by the Max Planck group[7] and represents the liquid as a collection of spherical particles interacting with various Lennard-Jones 6-12 potentials. The amphiphilic (surfactant) molecules are made of 5 particles - beads connected by chemical unbreakable bonds into a single chain. One

terminal bead is the hydrophilic head, the remaining 4 beads form the hydrophobic tail. This model also goes by the name of "coarse-grained" model and is a simplification of the so-called "Martini force field"[8]. Therefore we use molecular units related to the model and the potential used; in particular the collision diameter σ and the depth of the potential minimum ϵ . Thus the reduced temperature is $k_B T/\epsilon$.

Section 1. Structure Factor and Bulk Correlations.

The fluctuation spectrum often termed the "structure factor" $S(q)$ is an average height-height correlation; the very concept originates from a theoretical picture. In the theory, a bilayer or membrane is pictured as an infinitely thin sheet - a mathematical surface - embedded in three dimensions, initially flat "at rest" or "at equilibrium". For small deviations from that state, the state of the surface is fully given by a function $h(x, y)$. The height h is measured along the z -axis and $z = z_0$, i.e. $h(x, y) = z_0$ is the reference flat state. The requirement is that for every x, y the height $h(x, y)$ be unique, i.e. $h(x, y)$ cannot be a multivalued function. Fluctuations, due to thermal motion, are then described by the correlation $h(\mathbf{R}_1)h(\mathbf{R}_2)$. In a translationally invariant system, the latter reduces to a function of the relative distance vector \mathbf{R}_{12} and that is Fourier-transformed to become $S(q)$ on averaging. Here \mathbf{R} stands for position vector in the (x, y) plane and $\mathbf{q} = (q_x, q_y)$.

Of course no membrane nor bilayer is infinitely thin; wobbling and undulations of the surface position $h(x, y)$ are not the only source of fluctuations. A fuller description of the fluctuations in any liquid is provided by the density-density correlation function

$$H(1, 2) \equiv \langle \rho(1)\rho(2) \rangle, \quad (1)$$

with density $\rho(\mathbf{r})$, abbreviating $\mathbf{r} = (x_1, y_1, z_1)$ to (1) etc. For nearly planar bilayers, exploiting translation invariance and taking the Fourier transform w.r.to the \mathbf{R}_{12} variable results in a function of three variables $H(z_1, z_2; q)$. This function in inhomogeneous systems with planar interfaces or wetting layers has been extensively investigated[9,10,11,12].

The height fluctuation spectrum $S(q) = \langle h_q h_{-q} \rangle$ is but a projection of the density-density correlation function:

$$S(q) = \int_0^L dz_1 \int_0^L dz_2 (z_1 - z_0) H(z_1, z_2; q) (z_2 - z_0) \quad (2)$$

Besides providing a check on the direct computation, this route is instructive because it demonstrates that $S(q)$ is a projection of H which, as we know, contains bulk density fluctuations and short range correlations. Indeed in a homogeneous system H reduces to the Fourier transform of the radial distribution function $g(r)$ (plus an unimportant term). It was obvious[4,5] that, besides the small- q asymptotics of bending-cum-capillary waves, the traditional $S(q)$ must contain contributions from ordinary density

fluctuations present in all liquids. That it is so the nearest-neighbor peak[4,6] in $S(q)$ tells us. But to see it, a sufficiently wide range of q must be included in the computation of S .

In simulations one deals with particles for which the microscopic density is defined as the sum of Dirac delta-functions

$$\rho(x, y, z) = \sum_{j=1}^N \delta(x_j - x)(y_j - y)(z_j - z) \quad (3)$$

where j is the particle index. This is converted to $\bar{\rho}$ obtained as the number of particles in a given box (bin) of arbitrary size; formally it is obtained by integration over the box size. So far we have limited the sum to particles $j \in (1, N)$ being the beads "a" that is the heads of the amphiphilic molecules, also distinguishing the "upper" from the "lower" monolayer. In principle one can construct and compute the head-solvent (a-s), head-tail (a-t), and tail-tail (t-t) correlations but this has never been done so far.

It is well known that $S(q)$ diverges at $q = 0^+$ showing in a spectacular way the existence of capillary waves as $(1/q^2)$, possibly augmented by the bending contribution $(1/q^4)$ [13]. What happens with the increase of q is not so well understood. In much of work only a small range of q was explored; an exception[4][6] with larger range revealed several features. Fig.1 shows recent data, of the same qualitative shape. After the initial fall, S goes through a minimum near $q^2 \sim 1$. and raises to a series of peaks, the first one located near $q = 2\pi/\sigma$, where σ is the collision diameter, our unit of length. Hence the first peak is the nearest-neighbor peak, very much like the n.n. peak of the bulk structure factor.

The existence of a minimum presents a temptation to represent S as a sum of a decreasing and an increasing term. One would be the asymptotic divergent contribution of undulation waves, the other would be the contribution of bulk-like fluctuations, culminating in the nearest-neighbor peak.

An excellent idea is now borrowed from Reference [6] where besides S , the average with unity replacing h was extracted from simulation. This was deemed to represent the bulk-like fluctuations[6]. Formally, we obtain this function by integrating the density-density correlation function H over the z -variables without the h factors. There results the generalized susceptibility, already introduced [12] in the context of undulating liquid surfaces. First

$$\chi(z_1, q) = \int dz_2 H(z_1, z_2; q) \quad (4)$$

and then

$$\chi(q) = \int dz_1 \chi(z_1, q) = \int \int dz_1 dz_2 H \quad (5)$$

Thus

$$\chi(q) = \langle \sum_j \sum_m \exp[i\mathbf{q}\mathbf{R}_{jm}] \rangle \quad (6)$$

In the context of an interface in an external field, χ can be interpreted as a susceptibility, but here it represents a certain projection of the bulk fluctuations of the liquid bilayer.

Subtractions, i.a. of $S(q) - \chi(q)$, were also investigated [6]. In Fig.2 and 3 we show the results of such subtraction for the smoother version of S *i.e.* with S of individual monolayers and with floating ("recentered") local reference planes. The susceptibility $\chi(q)$ is fitted to a scaled and shifted Lorentzian about the n.n. peak. The capillary-wave asymptote has not been subtracted hence it persists at $q \rightarrow 0$. The difference is not nil, but even without fine-tuning the shapes show this is the right track - the bulk contribution is dominant and $\chi(q)$ is a close representation of it. One may think this fit remarkable.

The computation of S from simulation involves a certain detail[6] about the choice of reference plane $z = z_0$ from which $h(x, y)$ is measured. For a system bilayer+solvent confined to a simulation box $L \times L \times L_z$, the obvious "absolute" coordinate system has the corner of the parallelepiped as its origin. Let the position of the surface be given by $h(x, y)$. Then the flat reference state is $h(x, y) = z_0$; the issue arises what is our choice for z_0 ? [6]. Briefly, it can be the middle (plane) of the bilayer z_{mid} or a middle (average) plane of either monolayer, \bar{z}_1 or \bar{z}_2 , each either constant throughout the simulation run (*i.e.* constant in "time") or calculated afresh at each time t (*i.e.* "recentered" or "floating"). Explicitly then

$$z_{mid} = \frac{1}{N} \sum_{j \in a} z_j \quad (7)$$

and similarly for z_1 or z_2 with the sum limited to one monolayer. In our work we used the floating individual reference planes z_1, z_2 for each monolayer - in most cases. These choices were discussed and investigated in detail[6]. That the choice matters is proven by Fig.1 which shows $S(q)$ computed in the same run with recentered $\bar{z}_1(t)$, $\bar{z}_2(t)$, and $z_{mid}(t)$. For the first two S coincide (as might be expected) but the last shows a transition from the undulation regime to bulk fluctuation regime much better

displayed. Such an abrupt change is therefore a universal feature as it was seen with two other models of intermolecular forces[6] and now with our version of the "coarse-grained" model. The region of q where S raises towards the n.n. peak, corresponds in the bulk liquid to distances *larger* than the n.n. distance and therefore to many peaks in the r.d.f. $g(r)$. The three-dimensional Fourier transform $g(k)$ of the bulk liquid $g(r)$ is smooth just as $S(q)$ is in that region.

We have also investigated the shape of a function of q calculated by the same recipe as S but for a slab of homogeneous liquid of spherical free particles (a) with 120000 particles at high density $\rho = 0.9$ and with periodic boundary conditions or (b) immersed in a larger cube of the same liquid. In (b) boundaries of the slab were ghosts so that the slab was an open system with a fluctuating number of particles. For a thickness of 6 (and z_0 constant in the middle of the slab), we obtained $S(q)$ of the same shape as the Percus-Yevick $1/(1 - \rho c(q))$ curve shown in Fig.4. Also $S(q)$ (weighted by $(h - z_0)$) and $\chi(q)$ (not weighted cf. eq.(5-7)) differed very little in shape. See Fig.5. Such structureless background with only nearest-neighbor peak ought to remain if the capillary-wave contribution is subtracted from full $S(q)$. This exercise also showed that $\chi(q)$ was very close to these quantities obtained for a homogeneous liquid.

A technical detail is that when we compare $S(q)$ or any other quantity derived from $h(x, y)$ for different reference planes, the difference between two correlations $< X(q)X^*(q) >$ (where asterisk denotes a complex conjugate) and $< Y(q)Y^*(q) >$, can be converted to $< (X - Y)(X - Y)^* >$, but the mixed term $< X^*Y > + < XY^* >$ must be included.

As mentioned in connection with the theory of scattering off surfaces[14], the average $< (h(\mathbf{R}_1) - h(\mathbf{R}_2))^2 >$ is invariant with respect to the choice of reference plane and is equal to $< h(R)^2 > - S(R_{12})$; the invariance of $S(q)$ follows for $q \neq 0$. Because of imperfect orthogonality of the Fourier coefficients, the $S(q)$ from simulations was not invariant.

There exists a method of computing Fourier coefficients with perfect orthogonality; it has been employed[15] for computation of the average area of the fluctuating bilayer $A > L^2$ and in a calculation of the areas and curvatures[16]. An illustrative example can be found in the Appendix B. Given N coordinates r_j interpreted as $x_j, y_j, h(x_j, y_j)$ we choose a number $n = 2m + 1$ and construct the Fourier finite sum

$$h(\mathbf{R}) = a_0 + \sum a_m \cos(\mathbf{q}_m \mathbf{R}) + b_m \sin(\mathbf{q}_m \mathbf{R}) \quad (8)$$

with the set of twodimensional q -vectors arbitrarily predetermined, *e.g.* filling a half of a square centered on $(0,0)$. The coefficients a_m, b_m are then determined by the least-square fit of h to $N > n$ particle coordinates. The price one pays for the perfect orthogonality is the limited number of q 's; at $n = N$ the function $h(x, y)$ becomes an interpolating polynomial and this is not what one wants. In practice $n = 2m + 1$ ought to be significantly smaller than the number N of points to be fitted. An example of computed curvature is given in Appendix B.

1A. The asymptotics of $S(q)$.

A quantitative description of $S(q)$ for vanishing q is provided by the capillary-wave theory which has been formulated and derived in a variety of ways (see *e.g.*[10]) and predicts $S_{cap}(q) = (kT/A)(1/(D+\gamma q^2))$. Here D stand for the external-field contribution, A is the nominal (projected) area, $\beta = 1/kT$, and γ is the true full macroscopic[10] surface tension. On the other hand the very successful mesoscopic bending hamiltonian was combined with the above result[13]. In the absence of an external field ($D = 0$)

$$S(q) = (kT/A)(1/(\gamma q^2 + \kappa q^4)) \quad (9)$$

with κ the bending (rigidity) coefficient.

We rewrite (9) as

$$f(z) = 1/(\gamma z + \kappa z^2) \quad z \equiv q^2. \quad (10)$$

Besides the obvious pole at $z_1 = 0$ there is another pole at $z_2 = -\gamma/\kappa$. Normally $\gamma > 0$, $z_2 < 0$ and is outside the range of z , $z \geq 0$. However, when we extended our simulations to the entire bilayer isotherm[4], we found a crossover transition to a floppy state (at areas smaller than that of the tensionless state), where γ is negative. Then the pole z_2 has moved to the positive part of the real axis and, as a result, $S(q)$ diverges *not* at $q = 0$ but at $q^* = \sqrt{z_2} = \sqrt{|\gamma|/\kappa}$.

This finding[4] qualifies the standard statement about the divergence of the fluctuation spectrum *vel* structure factor $S(q)$. It is only in the extended state with positive Γ that S diverges at $q = 0^+$.

Splitting $f(z)$ in partial fractions, we find

$$((z_1 - z_2)f(x) = \frac{1}{(z - z_1)} - \frac{1}{(z - z_2)} \quad (11)$$

Thus the q^{-4} dependence is an illusion outside the tensionless state. At the tensionless state the two poles merge and the asymptote is a pure $1/z^2 = q^{-4}$.

The standard expression(9-10), proposed heuristically[13], found a support from a theory[17] starting from a microscopic bending hamiltonian. There κ is given; γ appears as a derived quantity. That calculation can be applied[2] to the height-height correlation $S(q)$ and in all versions invariably the general form (9) results(in [2] as based on[17]). Either the intrinsic area of the membrane is assumed constant, or microscopic elasticity is added, either there are three areas, four, or only two - always a form (9) is obtained, asymptotically at the saddle-point it must be admitted[17, 2, 16]. There seems to be no escape from it; unless if the theory would dispose of its basic picture of a single infinitely thin mathematical surface.

The standard expression(9) does not work well as a fitting equation for the simulation data of $S(q)$ at non-vanishing lateral tension Γ , even at apparently small q where other (bulk-like) contributions are supposed negligible. If $\Gamma > 0$ also $g > 0$ where we denote by g the value of γ obtained from a least-squares fit to S . Then at $q \rightarrow 0^+$, γ wins and $S \sim 1/z = 1/q^2$. But adding a positive $\kappa q^4 = \kappa z^2$ term to the denominator makes S smaller, i.e. would force the curve downwards with the second derivative negative - whereas the experimental S goes gently up above $1/z = 1/q^2$. And κ must be positive if it is to be a valid bending coefficient. These defects are apparent as elucidated below.

The apparent difficulties with (9) are displayed in the plot of the inverse, $1/S$ against $z = q^2$. The data were for $T = 1.35$, $a = 1.888$, $L = 40$, $N = 1800$ and importantly $\Gamma = 1.16$. With such large Γ , γ in eq.(9) will be positive. Therefore the curve following the data points, after starting linearly with positive slope should curve *upwards* because $\kappa > 0$ and yet it did curve downwards. Then we plotted $1/zS(z)$ against z ; this is Fig.6. Here we can identify the very small linear part, $\gamma + z\kappa$, which agrees with eq.(9). The point is that this range is very small. Having estimated the slope κ and the origin γ we go back and add the line $z\gamma + z^2\kappa$, to the plot of inverse $1/S$; this is Figure 7. The data agree with the theoretical prediction, but within a very small range of $z = q^2$.

So the theoretical expression (9) *can* be used and applied, but its range of validity is extremely small - in the Figures essentially up to the first two points. Further points are "spoiled" by the non-negligible contribution of bulk-like density fluctuations which raise S and put down $1/S$.

In all discussion so far we have used the notion of "the average". By the symbol $\langle \dots \rangle$ we mean a thermal average according to a (appropriate) Gibbs ensemble equivalently

a "time" average over the simulation run; if t is the index of a successive configuration of particles and there are T such steps, then

$$\langle X \rangle \equiv \frac{1}{T} \sum_t X_t \quad (12)$$

At a given step t we can introduce another average, that over particles; an example is an average z -coordinate of all particles

$$z_{mid} = \frac{1}{N} \sum_j z_j \quad (13)$$

which we take as the floating reference plane $z_{mid}(t)$. The notation $\langle \rangle$ does not refer to such subaverages at a given time step.

The empirical subtractions have not shown any apparent protrusions either in this work or earlier[6]. We therefore abandoned any further search for their signature in $S(q)$ and examined other possibilities.

B. Several Correlations and Protrusions. .

The density-density correlation H but an example of two-point correlations; we can define similar correlation functions for *any quantity* which can be attributed to a position in space or to particle j . Let it be C , its spatial density

$$C(x, y, z) \equiv \sum_{j=1}^N C(j) \delta(x_j - x)(y_j - y)(z_j - z) \quad (14)$$

Correlations H_{CC} will share several properties with the density-density correlation, notably its symmetry. We have produced several such correlation functions, mostly in our search for protrusions.

But before we move on to these complicated objects (functions of 3 variables) we show first results for several one-point functions.

An important observation is that a protrusion is a local irregularity of the *boundary* or transition region between the heads of a monolayer and the adjacent solvent. It has not much to do with the spatial distributon of heads, for which it is but a detail in the wing of $\rho_a(z)$. That is why it does not show, apparently, in the shape of $S(q)$. Fig.8 shows an example of the densities in this boundary region, for a low-temperature tensionless bilayer. Th solvent density $\rho_s(z)$ falls from its high value of 0.89204 intersecting the left wing of the (Gaussian with very slight asymmetry) density of heads in the "lower" monolayer. This merging of heads and solvent is a characteristic feature of the tensionless states; it is not always possible to point out to a sharp "boundary"; we deal with smooth change.

The derivatives $d\rho_a(z)/dz = \rho'_a(z)$ and $\rho'_s(z)$ are more specific; maximum or minimum may serve as the defined position of the head-solvent boundary. However, these quantities are averages over the plane (x, y) and thus will not uncover any protrusion. Better candidates are their fluctuations; off-hand one might suppose that with many protrusions forming and vanishing the fluctuation of ρ'_a ought to be larger and conversely. The second moment can be computed easily as an average over a simulation run for each z . We do not show these results because the protrusions did not show visibly enough.

The densitites are computed by counting the numbers of given species of particles in boxes (bins) thus producing a histogram, but the derivatives are not produced by numerical differentiation but by exploiting the *exact* relation between equilibrium

averages, known as the First Yvon Equation. It relates the spatial gradient of the first-order distribution function (density) to the average force on that point, e.g. for the x -component $(d/dx)\rho(x, y, z) = \langle F_x(x, y, z) \rangle$. Here F denotes the force acting on the volume element $dx dy dz$ about x, y, z . For our purposes this definition is transcribed to particle notation and in the simulation run we can make use of the forces, all calculated at each time step. Thus

$$d\rho_a(z)/dz = \langle \sum_{j \in a} F_z(j) \delta(z - z_j) \rangle \quad (15)$$

where $F_z(j)$ is the z -component of the total force acting on particle j and the brackets denote the ensemble average - in our case, average over time. The Dirac-delta localizes the particle j at z and this is routinely averaged over bins of chosen size (0.025 in all our runs). Checks with numerical differentiation not only showed agreement but also a superiority of the force calculation. The fluctuation of $d\rho/dz$ is then found from $\langle FF \rangle - \langle F \rangle^2$.

The large fluctuation in ρ' was an interesting and new quantity, but disappointing as a tool for detecting protrusions. Eq.(15), the first Yvon equation, suggests an examination of the *instantaneous* and/or *partly averaged* force and this thread was developed; some examples are shown below.

We have investigated several single-point quantities and their histograms $P(C)dC$, e.g. $C = \cos(\theta)$ where θ is the angle of \mathbf{F} , with the z -axis, $F_z = F \cos(\theta)$; either as an average over all pairs of chosen species, e.g. head-solvent,"a-s", or as the angle of the total force on particle "j". For angles, the position vectors are equivalently used. The wiggling of the boundary between the monolayer heads and the adjacent solvent ought to affect the histogram, along with the most-probable angle and the average angle.

Another possibility is to search for the coordinates x, y, z of this boundary. On the average, we obtain the density profiles and we can take the z -coordinate of the crossing of falling $\rho_s(z)$ with raising $\rho_a(z)$ as the definition of the position of the boundary. But the wiggling is gone on averaging.

We have tried more successfully to use the midpoint of the a-s \mathbf{r}_{ij} position vector of a-s pairs. Thus for each such pair $x_c = (x_j + x_m)/2$ with $j \in a, m \in s$ or conversely - with identical definitions for y_c and z_c . These c-points may be used to construct a surface, just as the positions of the heads are traditionally used to construct the surface representing the monolayer. But the distribution of their occurrence is also of interest. The histograms

$P(z_c)dz_c$ are shown in Fig.9 for a low temperature and with/without external field which smooths the boundary and ought to damp dynamically the protrusions. The external field (linear, derived from a double-well parabolic potential) sharpens P but also introduces a hump on top of the expected slight asymetry.

Having a set of positions x_c, y_c, z_c we can treat again the z -coordinate as a height and define the new S_c as

$$S_c(q) = \langle h_c(q)h_c(-q) \rangle \quad (16)$$

with

$$h_c(q_x, q_y) = \sum_j (z_c(j) - z_0) \exp[i(q_x x_c(j) + q_y y_c(j))] \quad (17)$$

and the sum over all c-points.

The resulting plot of S_c vs q has an entirely new shape. Fig.10 shows two cases: with and without external field. S_c picks up some capillary-wave contribution, which is correct and this is suppressed by the external field. Otherwise the field appears to have little effect on higher modes. Here the nearest neighbor peak does not appear at all. S_c always shows a definite hump in the interesting region of $q \in (1, 10)$ where protrusions are expected to enhance the fluctuation spectrum.

The small-gradient theory predicts[18,2] that the area increment is directly related to S , $\Delta A = A - L^2 = \sum_q A_q$ and $A_q = S(q) * q^2$. Accordingly, we computed $S_c(q)q^2$; the greatest increment of area precisely falls in the region of q where protrusions are expected, as shown in Fig.12. For comparison, Fig.11 shows the same data before multiplication by q^2 , *i.e.* it shows the series of $S_c(q)$. The series range from the floppy state to the most extended state of the bilayer isotherm, all at $T = 1.1$. Interestingly, the hump in Fig.12 does not change much with the stretching/compressing of the bilayer; the three states in the floppy region visibly differ from the rest by an overall raise at all q .

The idea of protruding heads leaving temporarily their environnement and venturing out into the neighboring solvent is in fact closely related to the concept of the roughness of a surface. Theory of equilibrium roughness (see e.g.[14]) of a surface, in particular of a solid, is related to the picture of two points on that surface and on the properties when their distance greatly increases. This view is corroborated by our results when the correlation S_c gave such promising results while the single-point fluctuations were

not very productive.

Summary.

New simulations are reported with an improved "coarse-grained" model and force field. A discussion is given of the bulk contributions to the ubiquitous fluctuation spectrum *vel* "structure factor". It is shown that in order to give any interpretation to the spectrum beyond the tiny asymptotic region, the range of Fourier vector must include the nearest-neighbour peak at $q \sim 2\pi/\sigma$, at the least[4][6]. The absence of any visible signature of the hypothetical protrusions, led to a search for such a signature at regions of space where these are supposed to occur, i.e. at the boundary between solvent and heads. Among many possibilities which are discussed, the new study of the head-solvent correlations appears very promising. The new correlation function S_c and the corresponding theoretical area increment are reported and a tentative interpretation in terms of protrusions is given.

ACKNOWLEDGEMENTS.

Several fruitful discussions with John F. Nagle (Pittsburgh) and Olle Edholm (Stockholm) are acknowledged. The interest of Professor Robert Holyst, the present Director of the Institute of Physical Chemistry of the Polish Academy of Sciences, is gratefully noted, and the financial support of the Institute is also acknowledged.

APPENDIX A

In the Appendix we give some details about the model and simulation procedure. The model we use was introduced by the Max Planck group[7] as an extension of the very first modelling of amphiphilic molecules as dimers in a solvent[18]. The simulated liquid system is made of spherical particles, which are either solvent molecules or beads connected in linear chains of small length common to all, of unbreakable (chemical) bonds, to form amphiphilic molecules. One terminal bead represents the polar bead and the remaining 4 the nonpolar hydrocarbon chain. The intermolecular energy is a sum of pair interactions which are cut and shifted 6-12 Lennard-Jones functions.

In general the symmetrical matrices of parameters require 6 energies $\epsilon_{\alpha\beta}$ and 6 collision diameters $\sigma_{\alpha\beta}$. Practically in all simulation work the collision diameters were taken the same for all particles. Often the energy parameters were made all equal[7,18,20,21] as well. Then, as one author noticed[20] the molecule was not amphiphilic any more. Most likely the sterical effects arising from impenetrability of beads, apparently ensured for bilayer stability.

Our model can be viewed as a simplified version of the "Martini force field"[8], also used under the designation of a "coarse grained" model [6]. The essential feature of an amphiphilic molecule is the permanent chemical bonding of two antagonistic groups - the hydrophilic (polar) head and the hydrophobic (non-polar) tail, most often a hydrocarbon tail. We denote the solvent particles as "s", the heads as "a" and the tail beads as "t". The intramolecular bonds are confined to the small neighbourhood of the bond distance by a potential well with infinite barriers. The intermolecular bonds are ss,sa,aa,st,at,tt and we take all σ 's equal and all ϵ 's equal in two groups; while $\epsilon_{tt} = \epsilon_{at} = \epsilon_{st} = \epsilon$, the other group has a stronger force field: $\epsilon_{ss} = \epsilon_{sa} = \epsilon_{aa} = AUG * \epsilon$, with $AUG > 1$. In this way the polar beads "a" and "s" are endowed with a stronger attraction. In all work reported here the value $AUG = 2$. was used. . The cutoff at distance $r = 2.5\sigma$ is common to all, except that the repulsion between $s-t$ and $a-t$ pairs is obtained by putting the cutoff at $r = 2^{(1/6)}$ (and therefore the shift at $+\epsilon$).

The Molecular Dynamics simulations were done in the canonical ensemble *i.e.* at constant T, V, N with Nose-Hoover thermostat, over 1-7 millions of time steps for sizes from 49000 to 121000 particles, 1800-4500 amphiphiles.

APPENDIX B.

Here is given an illustrative example of the curvature calculation with and without the small gradient approximation. As explained in the main text, for 2000 heads a reasonable number of fitting coefficients would be a half i.e. 1000 which means 500 q -vectors which translates to a square of 31 by 31 i.e. for $q_x = (2\pi/L)n_x$ we can have $n_x = 0, \pm 1, \pm 2, \dots, \pm n_{max}$ with $n_{max} \sim 15$. That is a limitation, for values of L used in simulations, nearest-neighbor $q_{nn} = 2\pi$ is beyond reach of this procedure. Already for $n_{max} = 4$ we have 81 by 81 matrices. After solving for the least-square Fourier coefficients, which has to be done in quadruple precision, the function $h(x, y)$ and its derivatives are computed as needed for the computation of integrals, like integral (or total) curvature

$$C = \int_0^L \int_0^L dx dy \sqrt{1 + p_x^2 + p_y^2} \mathcal{H}(x, y, p_x, p_y, ..)^2 \quad (B.1)$$

where the p 's are the first derivatives of h and the mean curvature \mathcal{H} is given by the standard expression in the Monge gauge in terms of first and second derivatives. Same expression with \mathcal{H} omitted gives the true area. Small gradient approximations were reasonably close as might be expected for computations with small n_{max} . Figure 13 shows the curvatures plotted against the areas for several n_{max} ; the fractal nature of the area might have been expected but the (total) mean curvature also follows the same trend. Near $n_{max} \sim L$ the period is of the size of the bead but we cannot reach that.

References.

- [1] J.F.Nagle and S.Tristram-Nagle, *Biochemica et Biophysica Acta* 1469, 159-195 (2000).
- [2] for a review of theory related to simulation (and some exotic correlation functions), see J. Stecki, *Advances in Chemical Physics* 144, Chapter 3 (2010).
- [3] R. Lipowsky and S. Grothaus, *Europhys. Lett.* 23, 599 (1993).
- [4] J. Stecki, *J. Chem. Phys.* 120, 3508 (2004).
- [5] J. Stecki, cond-mat archive Dec.10,2004; *J. Chem. Phys.* 125, 154902 (2006).
- [6] E.G.Brandt, A.R.Brown, J.N.Sachs, J.F.Nagle, and O.Edholm, *Biophysical Journal* 100, 2104 (2011) and Supplement. Where references to other work can be found.
- [7] R. Goetz and R. Lipowsky, *J. Chem. Phys.* 108, 7397 (1998).
- [8] S.J.Marrink, A.H.de Vries, and A.E.Mark, *J.Phys.Chem. B* 108,750(2003).
- [9] J. S. Rowlinson and B. Widom, *Molecular Theory of Capillarity* (Clarendon, Oxford), 1982.
- [10] R. Evans, *Adv. Phys.* 28, 143 (1979).
- [11] P. Tarazona and R. Evans, *Molec. Phys.* 54, 1357 (1985)
- [12] J.Steck, *J. Chem. Phys.* 103, 9763 (1995), *ibid.* 108,3788(1998).
- [13] W. Helfrich and R. M. Servuss, *Nuovo Cimento* 3D, 137 (1984); see also Helfrich, in *Les Houches, Session XLVIII, 1988, Liquids at Interfaces* (Elsevier, New York, 1989).
- [14] S.K.Sinha, E.B.Sirota, S.Garoff, H.B.Stanley *Phys.Rev.* B38,2297(1988).
- [15] A. Imparato, private communication.
- [16] J. Stecki, unpublished.
- [17] J.-B. Fourier, A. Adjari, and L. Peliti, *Phys.Rev.Lett.* 86, 4970(2001).
- [18] A. Imparato, *J. Chem. Phys.* 124, 154714 (2006).
- [19] B. Smit *Phys. Rev. A* 37, 3431 (1988)
- [20] A. Imparato, J. C. Shilcock, and R. Lipowsky, *Eur. Phys. J. E.* 11, 21 (2003).
- [21] J. Stecki, *J. Chem. Phys. Comm.*122, 111102 (2005).

FIGURE CAPTIONS

Caption to Fig.1

The $S(q) = \langle h.h \rangle$ correlations for $T = 1.35$ $L_x = 61.25$ $N \sim 4000$, $\rho = 0.89$, total 121000 particles, tail length 8. S for all heads shown with plus signs (reference plane as recentered average $z_{mid}(t)$). Otherwise either monolayer (crosses) with individual recentered \bar{z}_1, \bar{z}_2 . The $\text{const.}/q^4$ asymptote is shown with line. The remarkable break near $q^2 = 0.1$ is also present in individual monolayer S provided the reference plane is z_{mid} , constant or recentered.

Caption to Fig.2

The generalized susceptibility $\chi(q)$ due to bulk-like fluctuations is fitted to a scaled and shifted Lorentzian $f(q) = f_0 + a/((q - q_0)^2 + b^2)$ and subtracted from the full $S(q) = \langle h.h \rangle$. Even w/o fine-tuning, this fit proves the dominant role of bulk fluctuations in $S(q) = \langle h.h \rangle$. Bare S - plus signs, χ - crosses, f - line, and the difference - boxes.

Caption to Fig. 3

The subtraction of generalized susceptibility $\chi(q)$ from $S(q) = \langle h.h \rangle$. Plotted against q : $S(q)$ (floating reference plane for one monolayer) - with plus signs, χ - crosses, fit to χ by a Lorentzian - line, the difference - boxes. Clearly the bulk contribution to S follows the shape of χ . Arbitrary scale, forcing equality of n.n.peaks. Same data as Figs.1 and 2.

Caption to Fig.4

Correlation $\chi(q) = \langle \exp[ikR] \rangle$ for the bilayer shown with plus signs and for the slab immersed in LJ liquid - with boxes, plotted against q . The identical shapes show that bulk-like fluctuations produce χ in the bilayer. Bulk Percus-Yevick $S = 1 + \rho h = 1/(1 - \rho c)$ is plotted with the line. Density $\rho = 0.9$.

Caption to Fig.5

Fluctuation spectra for a homogeneous slab of $N = 120000$ L-J particles at $T = 1.1$ density $\rho = 0.89$. The reference plane is at $z_0 = L_z/2$. $\chi = \langle \rho \rho(q) \rangle$ - plus signs, $s = \langle h \cdot h \rangle$ - boxes, $s' = \langle h \cdot h \rangle$ - diamonds. s for all N particles, s' - open system within $L_z/4, 3L_z/4$. The corresponding quantities for $T = 5$ are shown with stars and differ surprisingly little from $T = 1.1$ data. The ordinate is $n_x^2 + n_y^2$ proportional to q^2 . The n.n.peak is damped by the logarithmic scale.

Caption to Fig.6

Inverses $1/zS(z)$ plotted against $z = q^2$ for bilayer (boxes) and two monolayers (plus signs and stars) with common reference plane $z_0 = z_{mid}$ recentered and monolayers with individual reference planes recentered (circles). The straight line is a best fit to all, of $g + \kappa z$, at $z \rightarrow 0$. Data are for $T = 1.35, L_x = 40., \rho = 0.89, N = 1800, a = 1.88889$.

Caption to Fig.7

Inverses $1/S(z)$ plotted against $z = q^2$, with labels as in Fig.5, with the parabola $g * z + \kappa * z^2$ obtained from the straight line of Fig.5. Extremely small range of validity of Eq.(9) is apparent. But valid it is.

Caption to Fig.8

Densities $\rho(z)$ and their derivatives $\rho'(z)$ in the lower monolayer, shown as follows: solvent - full line falls as error function, heads - full line and shaded vertically. $\rho'_s(z)$ line with small boxes, very accurately a gaussian. $\rho'_a(z)$ - full line (black) with positive and negative values. At this tensionless state at $T=1.1$ the boundary between heads and solvent is fuzzy and broad.

Caption to Fig.9

Histogram of the z -coordinate of r_c (see text) plotted against z for the lower monolayer; solvent is to the left (lower z) and heads to the right, tails largely outside the Figure. No external field - plus signs, with a linear external field - stars; with an external field also supporting an artificial protrusion - circles. For comparison the density profile of heads (scaled by an arbitrary factor) is shown with small boxes and shaded by vertical lines.

Caption to Fig. 10

The new correlation $S_c = \langle h_c \cdot h_c \rangle$ for one monolayer with floating local reference plane with and without external field, plotted against q^2 . $T = 1.1$, 1800 amphiphiles, near tensionless state. A weak external field from a double well parabolic potential damps capillary waves. See text.

Caption to Fig.11

The $S_c = \langle h_c \cdot h_c \rangle$ correlation with h_c the (Fourier component of) z -coordinate of r_c plotted against $x = q^2$. The series includes floppy states and most extended states near the breaching point. For details see Caption to Fig.12

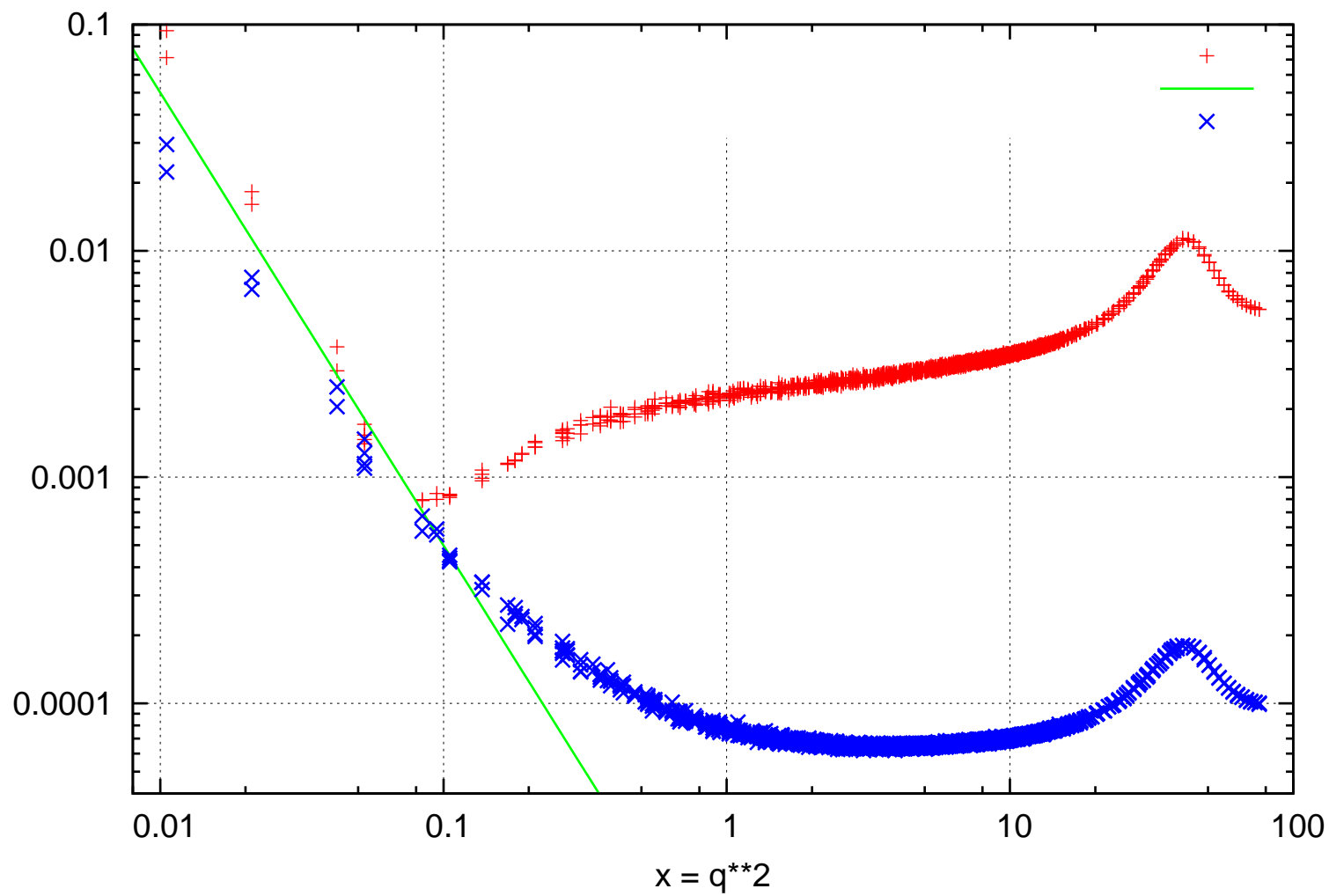
Caption to Fig.12

The $\langle h_c \cdot h_c \rangle$ correlation with h_c the (Fourier component of) the z -coordinate of r_c (see text) multiplied by q^2 and plotted against $z = q^2$. In the small-gradient theory the quantity $zS(z)$ is the q -component of the area increment dA_q . The successive curves are (in this order) for $L_x = L_y$ equal to 100. (label "1"), 97., 73.5 (label "3"), 64.0 ("4"), 62.5 ("5"), 61.25 ("6") 61.0 ("7") 60. ("8"). and 59. ("9"). The last three belong to the floppy region. An enhancement in the region $1 \leq q^2 \leq 10$ can be seen, largely independent of the area per head. $T = 1.35$, 121000 particles, 2000 heads in this monolayer. The area per head ranges from 1.7826 to 5.035.

Caption to Fig.13 (Appendix B)

For successively increasing numbers of Fourier coefficients ($M=12,40,112,364$) total (mean) curvature and area increment (over L^2) computed from the same data on 4000 heads by the method of Appendix B. Here ΔA is plotted against total \mathcal{H} . There is no saturation in sight. Each point in the cluster of data points results from one configuration of heads, taken successively from the same simulation run, at $T=1.35$, density 0.89 $L = 39$. 2000 heads in one monolayer.

FIG.1 S(q)



Fri Aug 26 20:35:38 2011

FIG.2

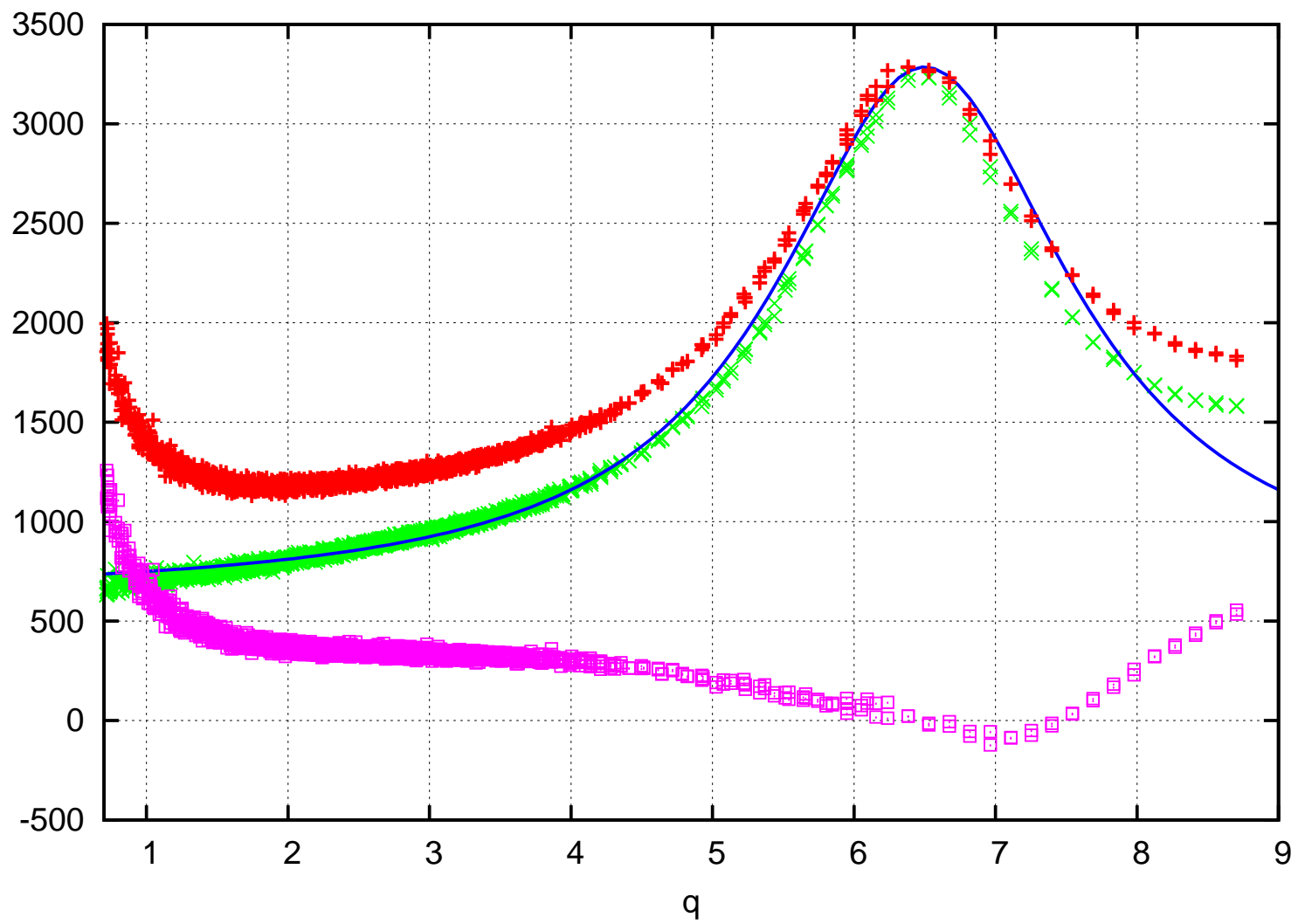


FIG.3

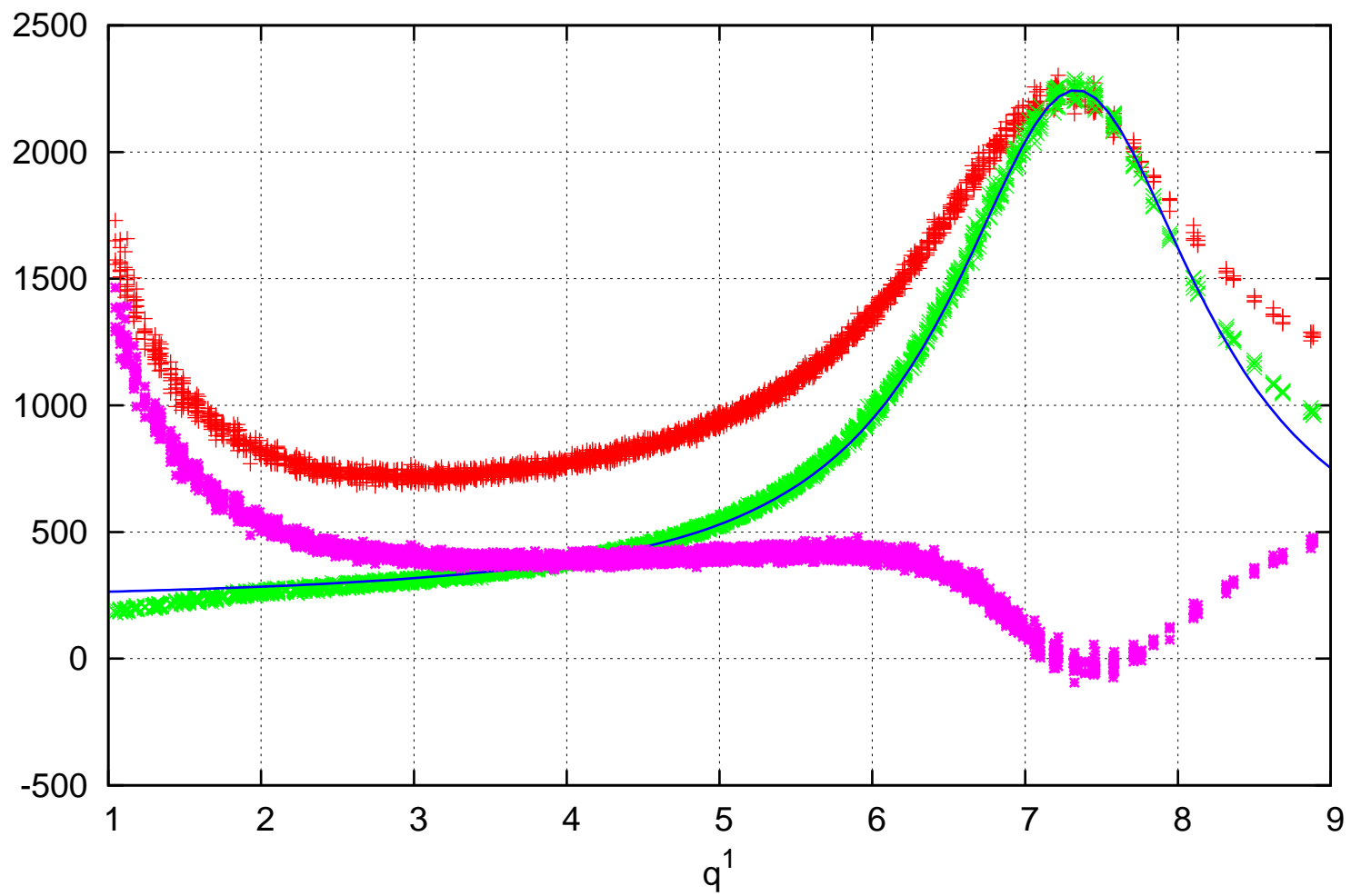
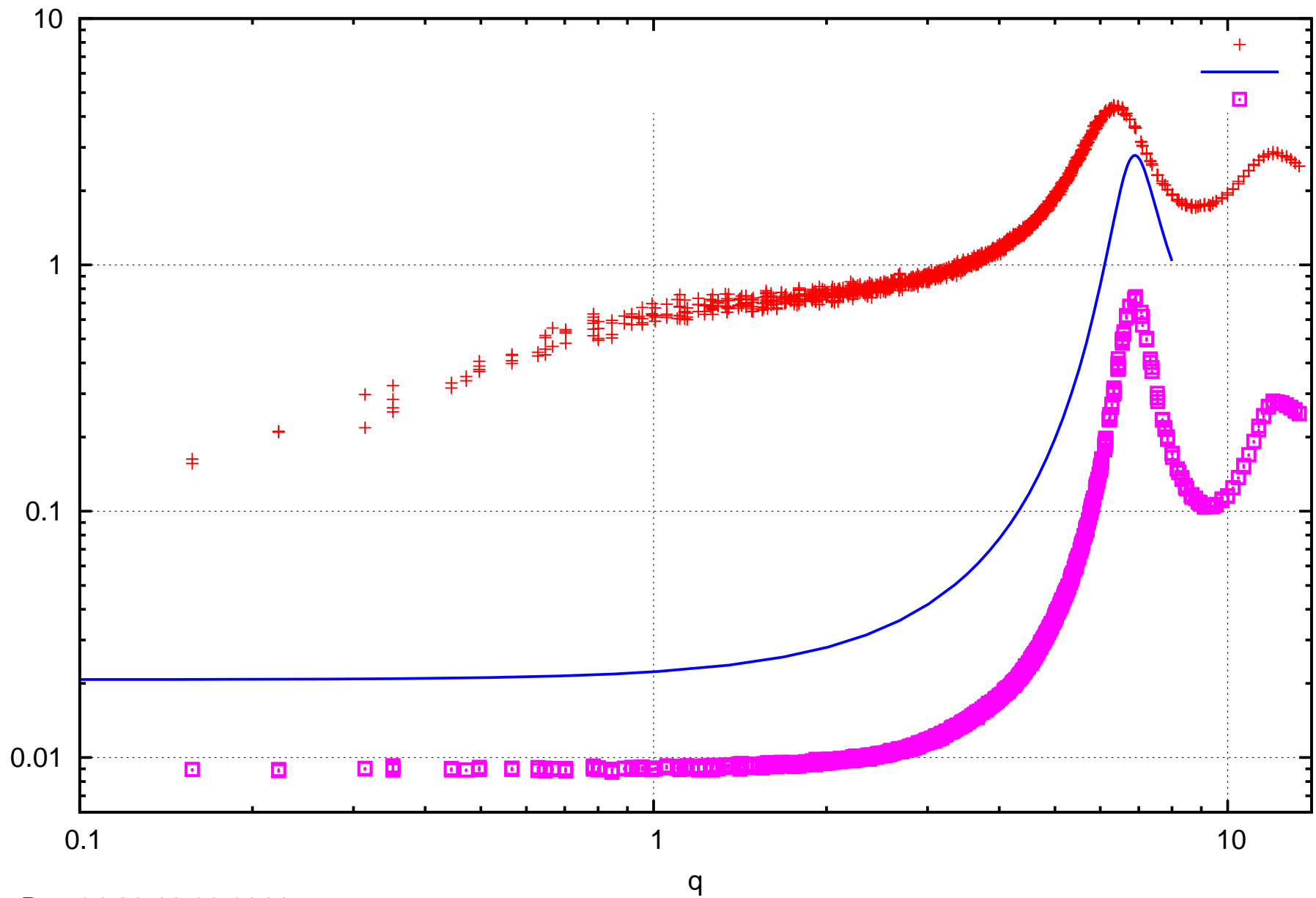


FIG.4



Sun Dec 04 22:12:23 2011

FIG.8

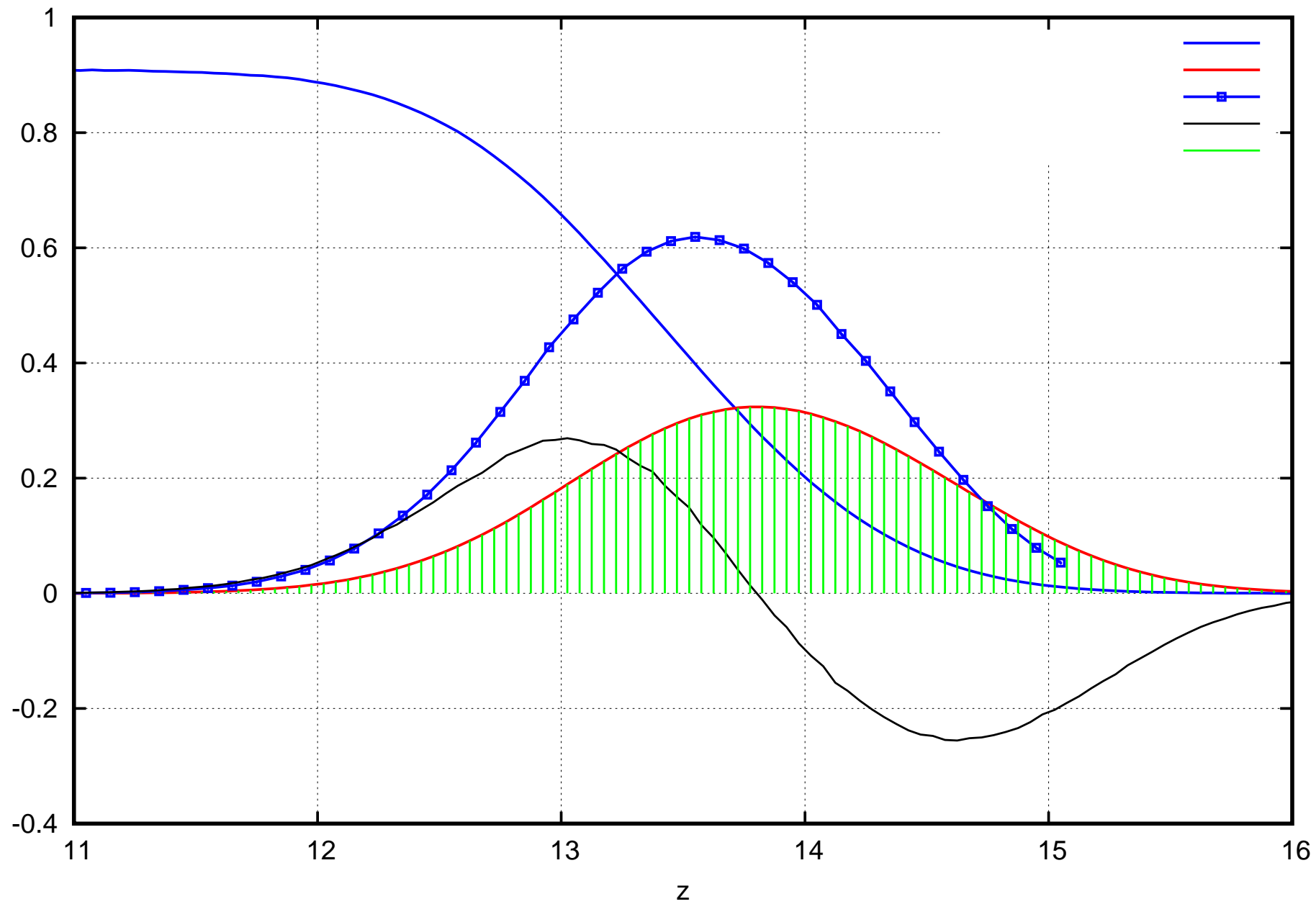


FIG.9

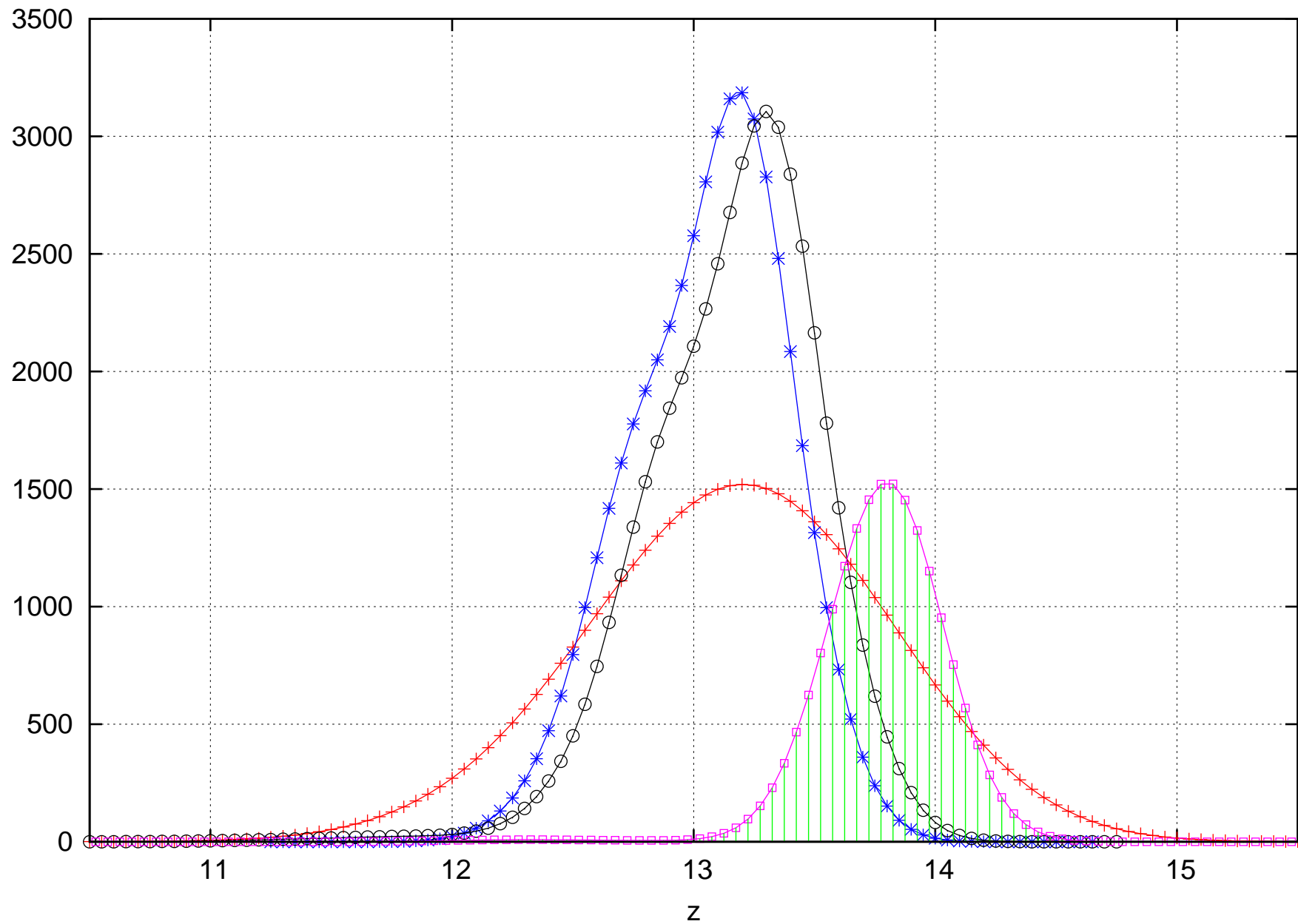
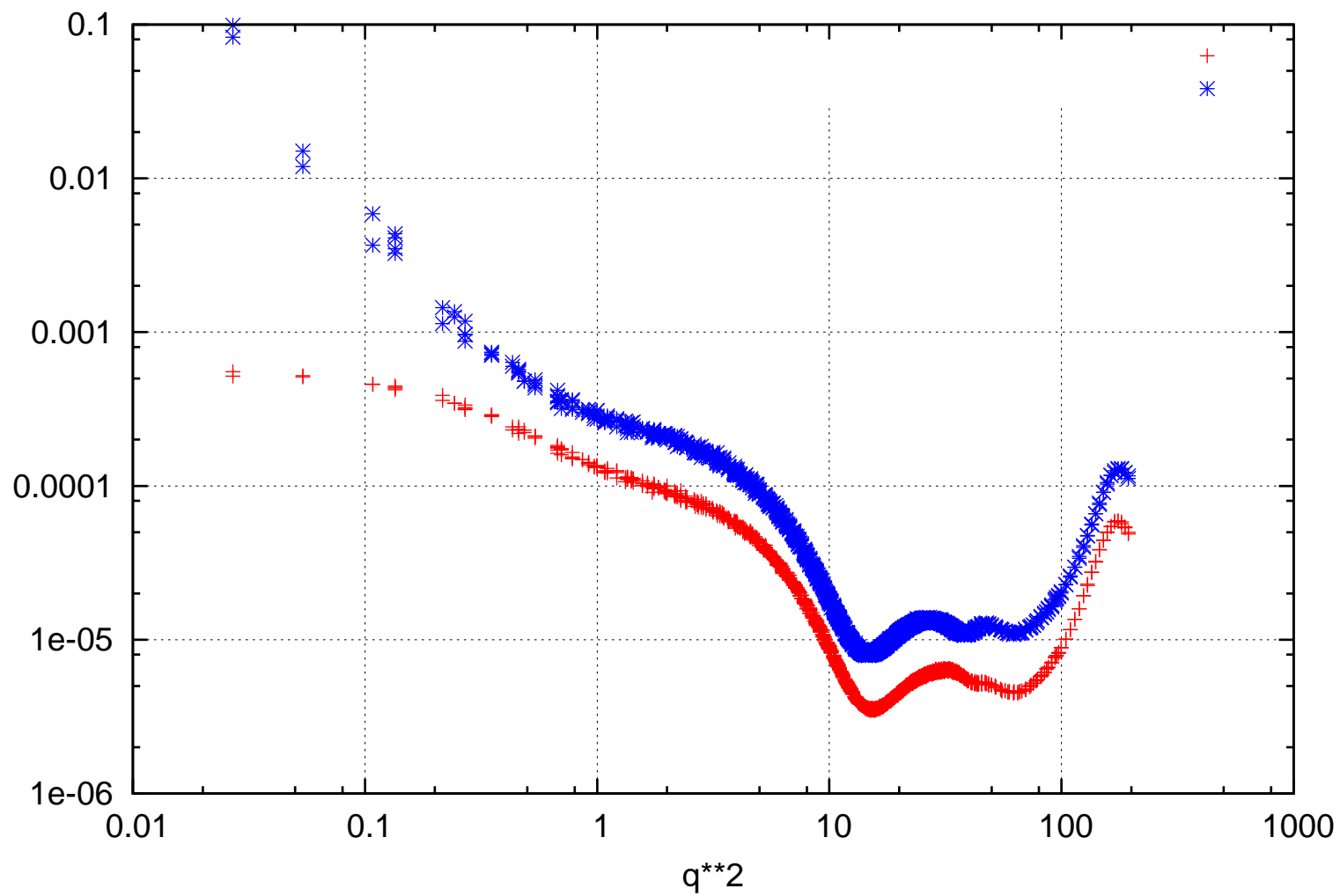
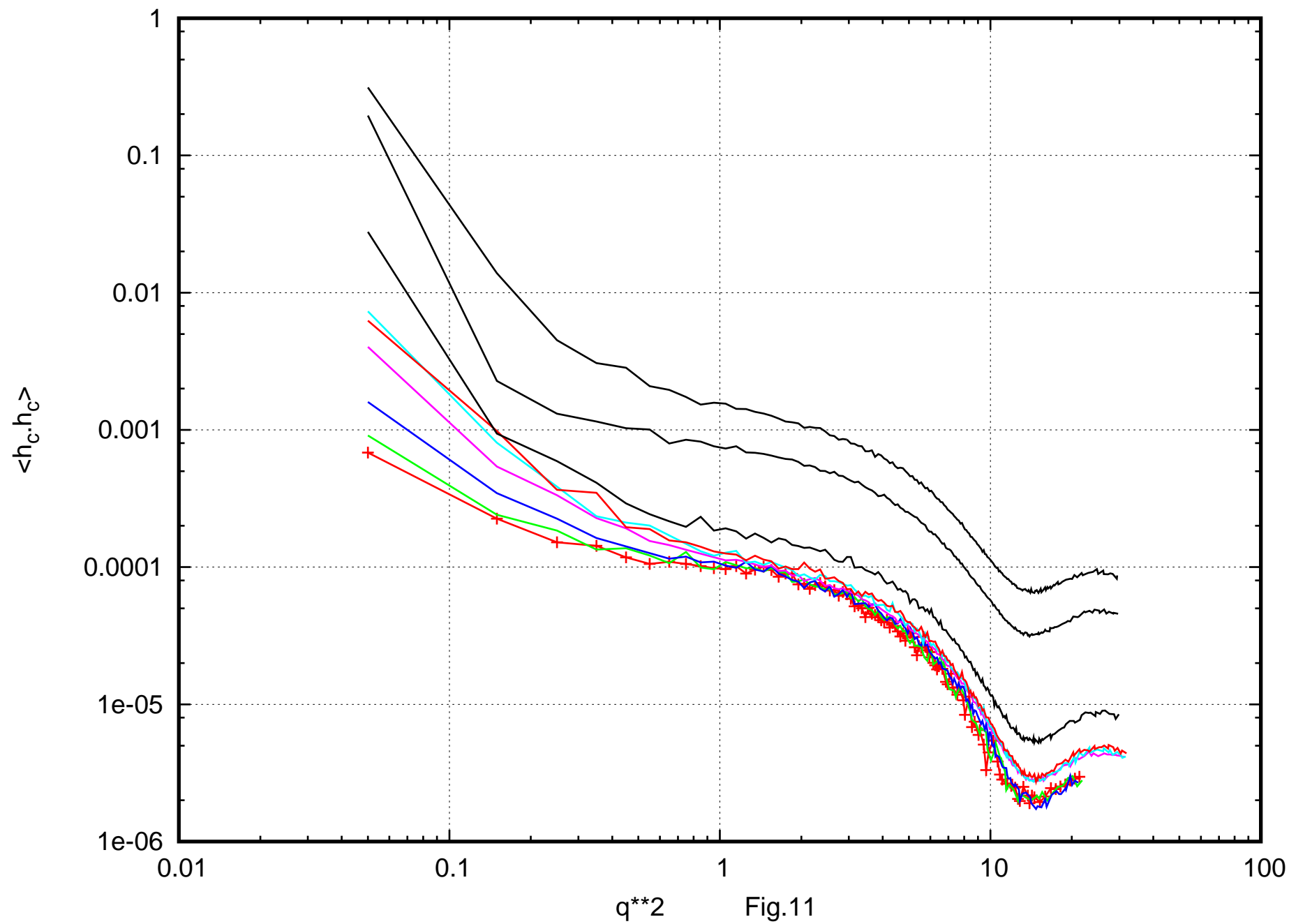
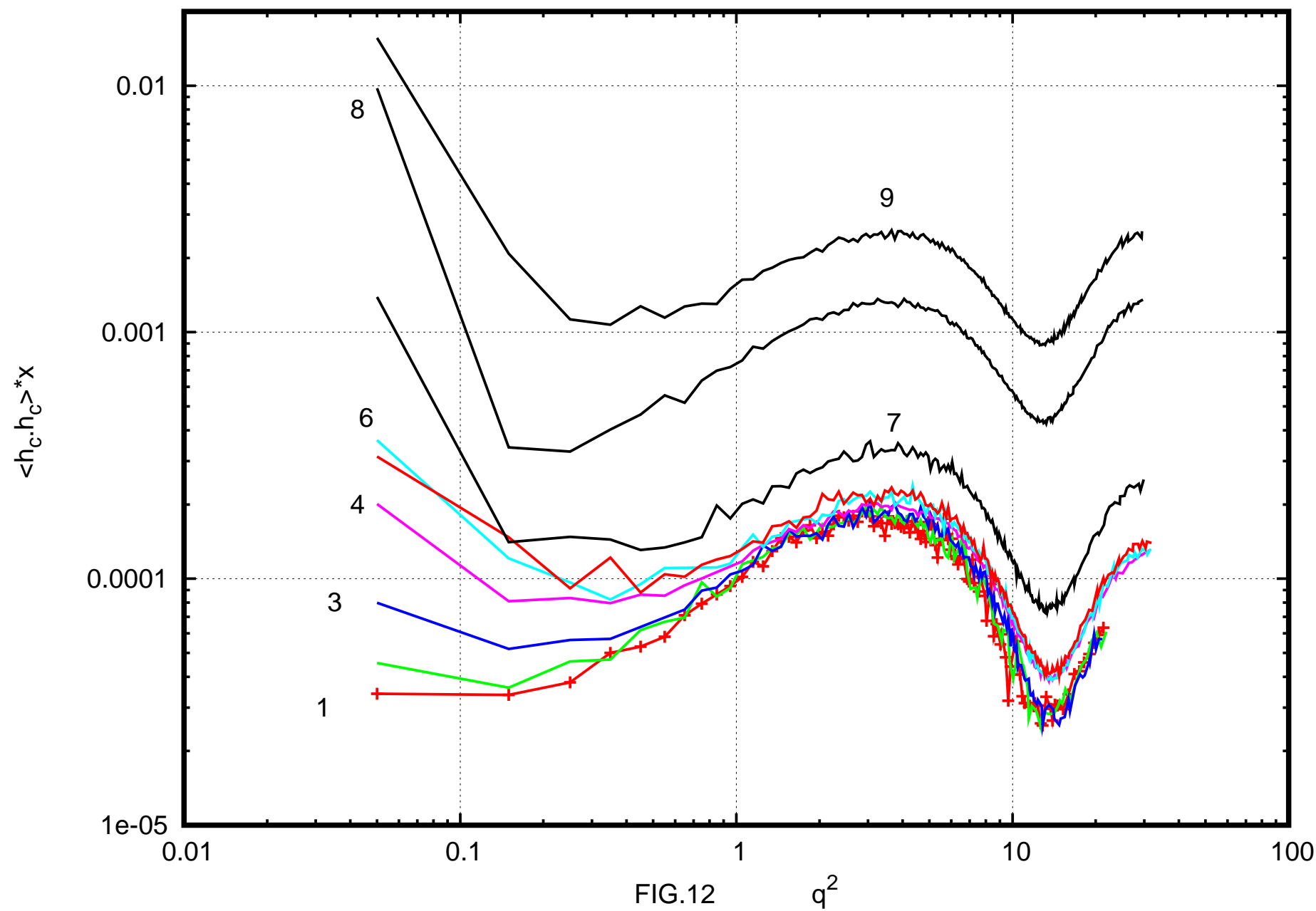


FIG.10



Thu Nov 10 00:08:20 2011





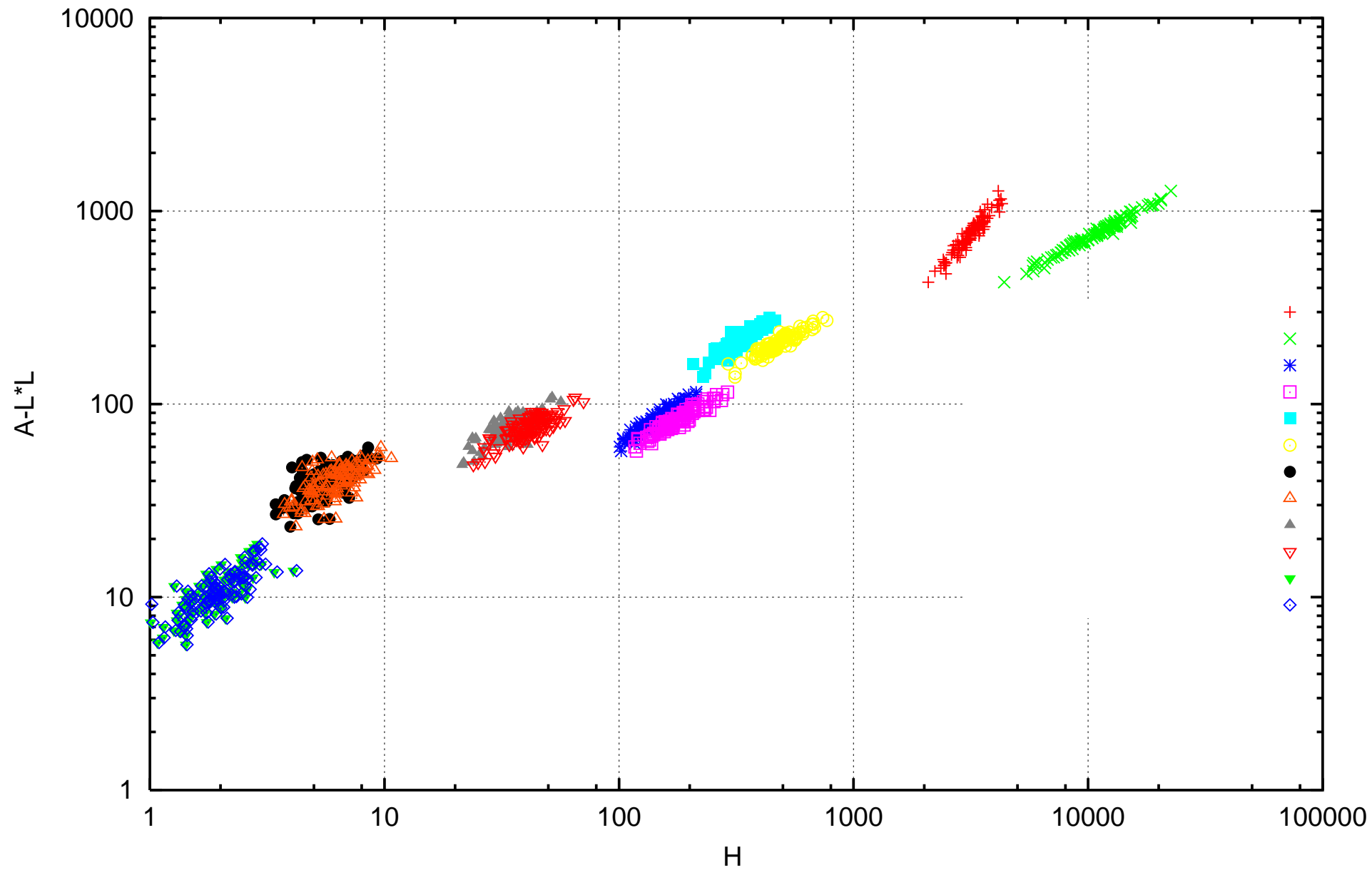


FIG.5

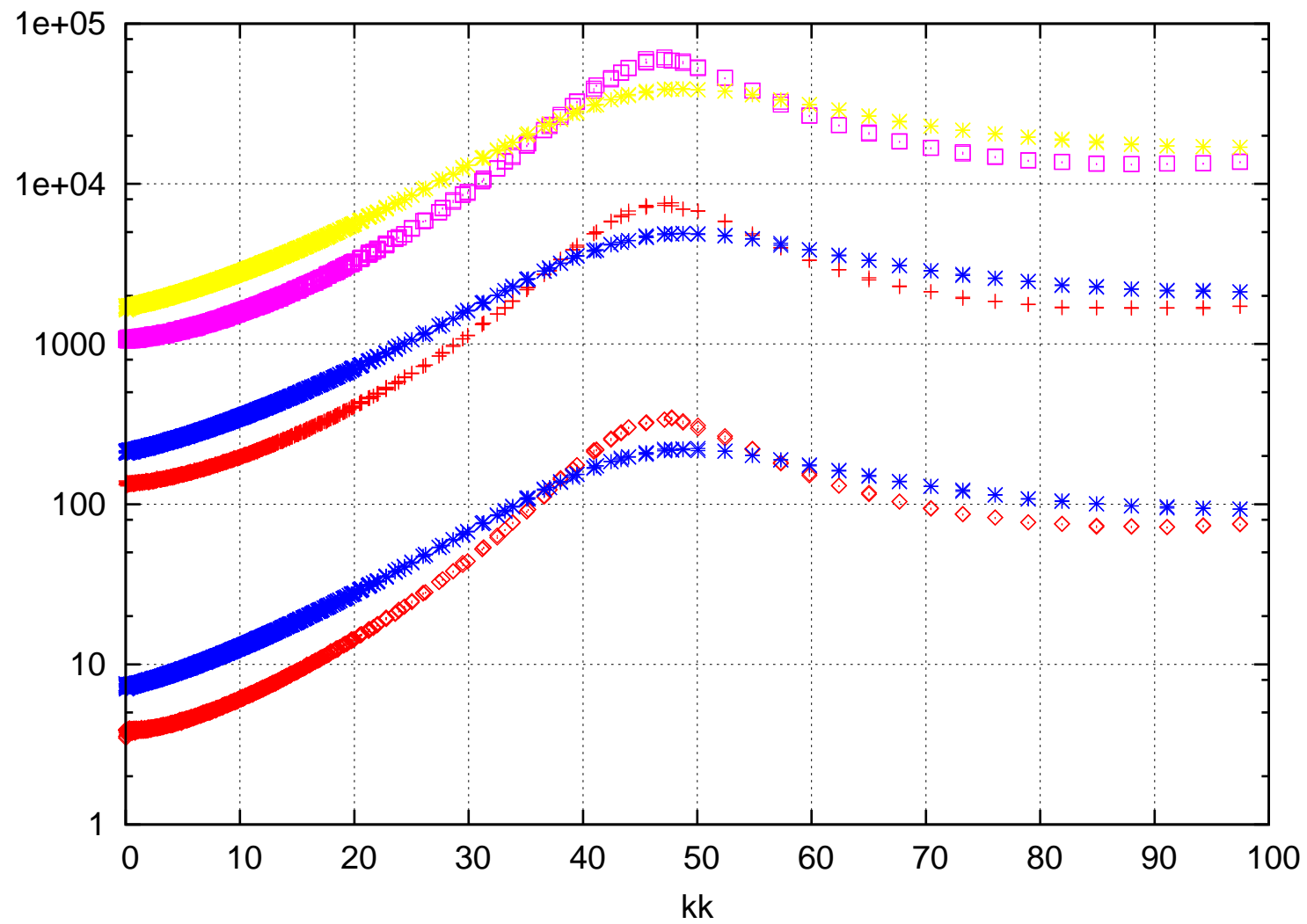




FIG.6.

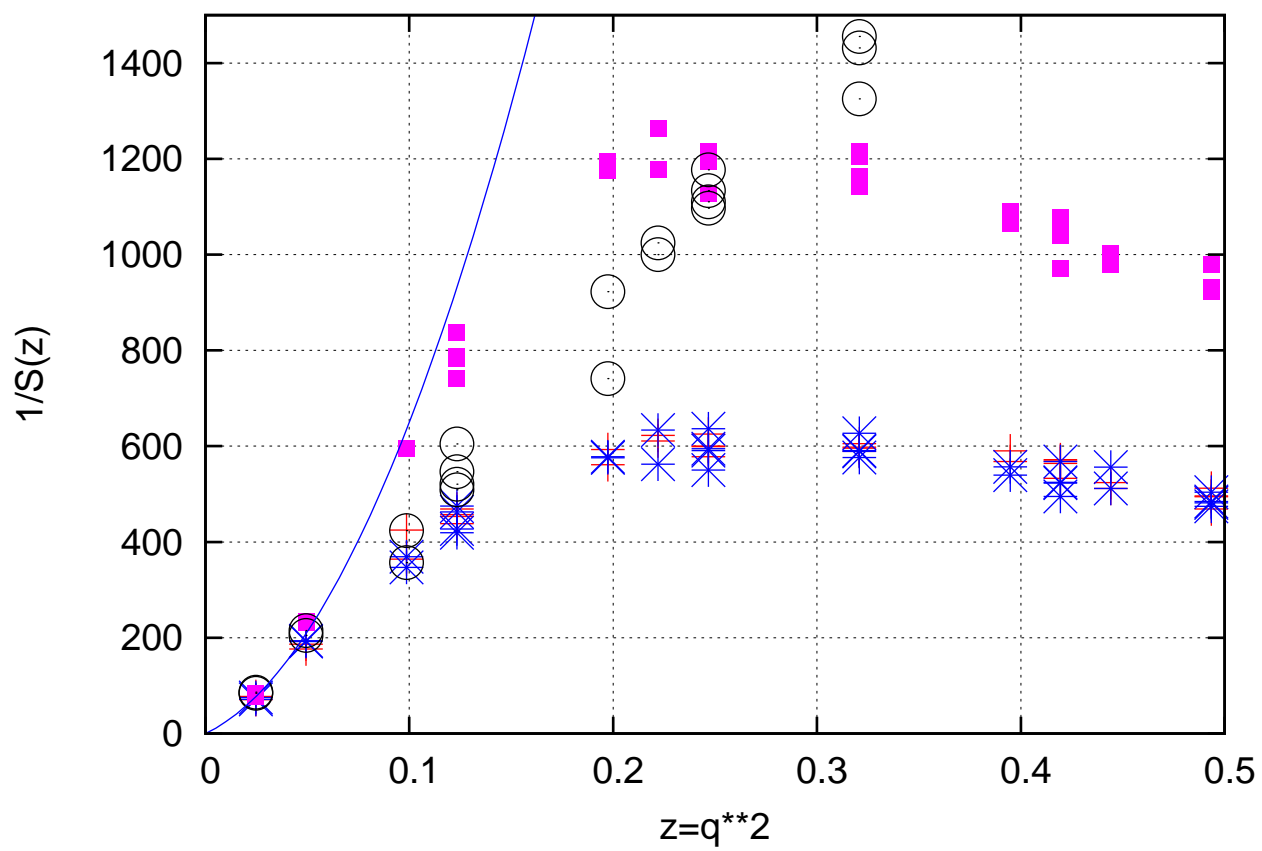


FIG.7.